

Modification of Thermal Chemical Rates in a Cavity via Resonant Effects in the Collective Regime

Jing Sun* and Oriol Vendrell*

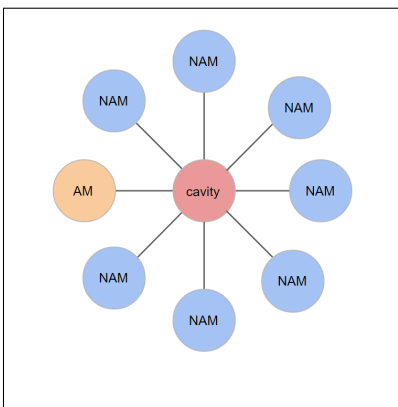
*Theoretische Chemie, Physikalisch-Chemisches Institut, Universität Heidelberg,
69120 Heidelberg, Germany*

E-mail: jing.sun@pci.uni-heidelberg.de; oriol.vendrell@uni-heidelberg.de

Abstract

The modification of thermal chemical rates in Fabry-Perot cavities, as observed in experiments, still poses theoretical challenges. While we have a better grasp of how the reactivity of isolated molecules and model systems changes under strong coupling, we lack a comprehensive understanding of the combined effects and the specific roles played by activated and spectator molecules during reactive events. In this study, we investigate an ensemble of randomly oriented gas-phase HONO molecules undergoing a *cis-trans* isomerization reaction on an *ab-initio* potential energy surface. Using the classical reactive flux method, we analyze the transmission coefficient and determine conditions that lead to accelerated rates within the collective regime. We identify two main mechanisms at work: firstly, spectator molecules enhance the cavity's ability to dissipate excess energy from the activated molecule post-reactive event. Additionally, the interaction between spectator molecules and the cavity gives rise to the creation of polaritonic modes. These modes then interact with the activated molecule at a shifted resonance frequency.

TOC Graphic



Vibrational strong coupling (VSC) is an active area of research within the field of polaritonic chemistry but the effect of Fabry-Perot cavities on molecular reactivity is still a poorly understood phenomenon. Under VSC, Fabry-Perot cavities can resonantly couple to the infrared active modes of molecules thus leading to Rabi splitting and the formation of vibrational polaritonic bands under infrared irradiation.¹⁻⁷ Additionally, an increasing number of experimental works have reported the modification of the rate of thermal chemical reactions inside the cavity in the dark, i.e. under coupling to background thermal radiation and vacuum fluctuations of the confined electromagnetic fields.⁸⁻¹⁴ These experimental results have prompted the development of various theoretical models to explain how cavities alter the ground electronic state structure and spectroscopy, and more recently, how they modify reaction rates.^{9,10,15-21} These models often consider a single molecule coupled to a cavity mode whereas, in strong contrast, 10^6 - 10^{12} molecules are collectively coupled to the cavity in actual Fabry-Perot resonators.²² As a result, in order to recreate the same Rabi splitting and overall light-matter coupling as in experiments, theoretical models must consider a single or a few molecules in the strong to ultra-strong coupling regime. In terms of chemical kinetics, closing gap between multiple molecules, each weakly interacting with the cavity, and a single strongly-coupled molecule remains an open question, although theoretical proposals that cleverly exploit the high symmetry in the Hamiltonian have been put forward recently.²³

Early attempts to understand the effect of cavities on thermal reactivity were based on transition state theories under the assumption that the main effects correspond to modifications of the potential energy barrier separating reactants and products.^{24,25} While this is conceivable in the single-molecule, strong to ultra-strong coupling regime, alterations to the potential energy barrier of individual molecules cannot play a significant role in the *collective* strong coupling regime. More recently, the idea that the cavity effects must be of a dynamic and more subtle nature has gained traction.^{21,26,27} Accordingly, the cavity modifies the energy redistribution pathways of the reacting molecules, thus facilitating or hindering the reactive process. Dynamical effects are comparatively small and can be captured as a

correction factor to transition state theories. This is in line with the experimental findings, which consistently demonstrate that the most substantial alterations in chemical rates reported thus far fall within a range of no more than one to two orders of magnitude (see e.g. Table 1 in Ref. 28 and subsequent references).

In previous work, we studied the isomerization reaction of the HONO molecule inside a cavity at room temperature under fixed orientation.²⁶ We established that the cavity affects the energy redistribution to and from the reactive coordinate during the reactive event, and that this effect occurs when the cavity couples to infrared-active molecular coordinates directly or indirectly involved in the reactive process. This results in relatively sharp modifications of the rate as a function of the cavity frequency. Full quantum calculations on model systems have also established sharp modifications of the reaction rate when the cavity is resonantly coupled to the reaction coordinate.²⁷ To the best of our knowledge, the simulations in Ref. 26 contained the first converged canonical reaction rate calculations on an anharmonic *ab initio* potential energy surface with full account of dynamical effects that were conducted for a molecule coupled to a cavity. From a detailed mechanistic perspective, there still remains the open question of how the molecular ensemble, together with the cavity, participates in the modification of the reaction rate. Notably, recent work based on a three-dimensional reactive model with up to several thousand molecules finds that the microcanonical survival probability of a unimolecular dissociation can be modified collectively by the cavity when it becomes resonant with the vibrational modes of the molecules, and it indicated that the spectator molecules participate collectively.²¹

In this work, we consider ensembles of freely rotating HONO molecules in the gas phase and explore the collective effects on the *cis-trans* isomerization reaction rate. The single-molecule coupling strength is chosen small enough such that an effect on the reaction rate is still seen for one single molecule, but such that the Rabi splitting is still small. The latter means that, under irradiation, no defined polaritonic bands are present. Under such conditions, we explore the situation in which the addition of molecules at a constant coupling

strength results in the appearance of vibropolaritonic bands. We can demonstrate numerically that, in this regime, the resonance of the single activated molecule with the polaritonic bands of the cavity-ensemble system results in the same effect as the direct coupling of a single molecule with the cavity mode. Moreover, we show in detail how the orientation of the activated and non-activated molecules may differ for optimal interaction with the cavity, and the resonance frequency may shift for the activated molecule due to its higher energy content.

Although the size of the considered molecular ensembles is still orders of magnitude away from the actual experiments in Fabry-Perot cavities, we choose an interaction strength that brings the system from a weak to a collectively strong coupling as a function of the ensemble size. Our simulations demonstrate the collective effect on chemical rates in the under-damped regime and explain how the cavity enhances the rate when more molecules are added to the system. Finally, key to our analysis is the fact that the single activated molecule (AM), the molecule undergoing the chemical reaction at a specific moment in time, and the $(N - 1)$ spectator or non-activated molecules (NAM) play fundamentally different roles in the collective mechanism.

Here, we briefly introduce the Hamiltonian of the molecular ensemble on non-interacting gas-phase molecules coupled to a single cavity mode

$$H = \sum_{l=1}^N H_{mol}^{(l)} + H_{cav} \quad (1)$$

where the molecular and cavity terms read

$$H_{mol}^{(l)} = \sum_{j=1}^{N_a} \frac{\mathbf{P}_j^{2(l)}}{2M_j} + V(\mathbf{X}_1^{(l)} \dots \mathbf{X}_{N_a}^{(l)}), \quad (2)$$

$$H_{cav} = \frac{1}{2} \left[p_{cav}^2 + \omega_{cav}^2 \left(q_{cav} + \frac{\lambda}{\omega_{cav}} \cdot \sum_{l=1}^N \boldsymbol{\mu}^{(l)} \right)^2 \right]. \quad (3)$$

Here $V(\mathbf{X}_1^{(l)} \dots \mathbf{X}_{N_a}^{(l)})$ denotes the ground electronic state potential energy surface (PES) of

the l -th molecule with Cartesian positions $\mathbf{X}_j^{(l)}$ and momenta $\mathbf{P}_j^{(l)}$. The *ab initio* PES was obtained by Richter et al.²⁹ at the CCSD(T) level of theory. Hence, each l -th molecule is considered in its ground electronic state under the Born-Oppenheimer (BO) approximation and interacting with the cavity via its field-free dipole-moment vector surfaces $\boldsymbol{\mu}^{(l)} \equiv \boldsymbol{\mu}^{(l)}(\mathbf{X}_1^{(l)} \dots \mathbf{X}_{N_a}^{(l)})$. Similarly to other studies and to facilitate comparisons, we introduce the coupling parameter $g = \lambda\sqrt{\hbar\omega_{cav}/2}$, which has units of electric field.

According to the reactive flux method for the classical rate constant,³⁰⁻³⁴ the *cis-trans* reaction rate is described as

$$K(t) = x_{cis}^{-1} \langle \dot{\tau}(0) \delta[\tau(0) - \tau^\ddagger] \theta[\tau(t)] \rangle, \quad (4)$$

where x_{cis} is the equilibrium fraction of HONO at the *cis* geometry, $\dot{\tau}(0)$ is the initial velocity of a phase-space point perpendicular to the dividing surface between reactants and products, and τ^\ddagger is the torsion angle corresponding to the transition state (TS) geometry. A corresponding diagram illustrating the reaction coordinate and the *cis* and *trans* configurations is found in Fig. 1 in the form of a Newman diagram with the central N-O bond perpendicular to the plane of the paper and at the origin of the (x, y) -plane. The Heaviside function $\theta[\tau]$ is one for the *trans* configurations, and zero otherwise. The brackets represent the thermal ensemble average over all trajectories, where a temperature of 300 K is considered for all calculations. In practice, one obtains the reactive flux when $K(t)$ reaches its plateau value.³³ In cases where a plateau value cannot be reached, for example for two potential energy minima separated by a one-dimensional barrier without any dissipation, a reaction rate cannot be defined in the sense of Eq. 4. Transmission coefficients and rate constants without a time argument refer to their plateau value, and $\lim_{t \rightarrow 0^+} K(t) = K_{TST}$, where K_{TST} can also be evaluated through Eyring's equation.^{35,36} $K(t)$ can be related to K_{TST} through the introduction of a transmission coefficient $\kappa(t)$, $K(t) = \kappa(t)K_{TST}$, where $\kappa(t)$ is in practice the quantity of interest obtained from classical trajectories.³³ The enhancement or suppression

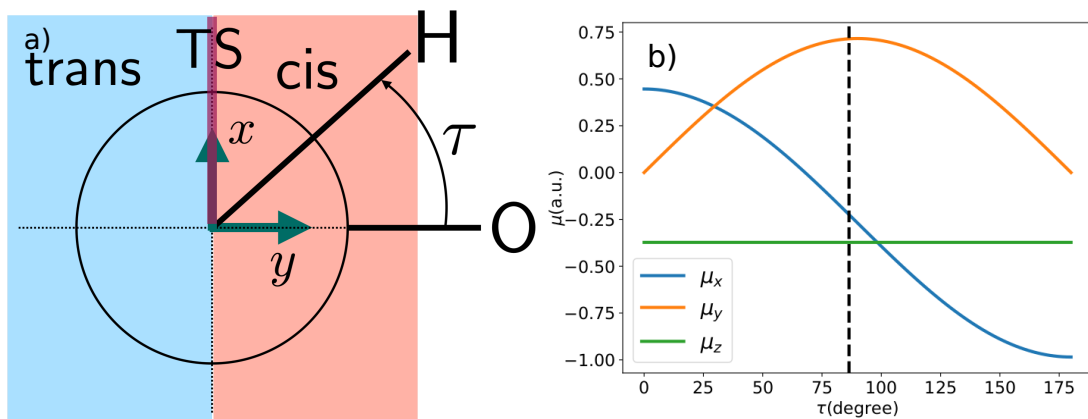


Figure 1: a) Newman diagram of the HONO molecule showing the definition of the body-fixed axes. The hydrogen atom is on the front side, the terminal oxygen atom is on the back, and the remaining oxygen and nitrogen atoms lie at the origin of the diagram along the perpendicular z -axis. The (y, z) -plane is determined by the ONO atoms, and the reaction coordinate τ corresponds to the dihedral rotation of the H-atom around the z -axis and on the (x, y) -plane. Its origin is set at the minimum energy configuration of the *cis* region. The transition state lies at about 90 and by symmetry also at about 270 degrees. b) Permanent dipole of the HONO molecule in atomic units as a function of the torsion coordinate τ . The axes are referred to the molecular frame axis.²⁶ The black dashed line represents TS.

of the reaction rate by the cavity can then be quantified through the comparison of the rate constant inside ($K^{(c)}$) and outside the cavity ($K^{(0)}$). Now, as long as the dividing surface between reactants and products is chosen to lie perpendicular to the cavity coordinate (cf. Fig. 3 in Ref. 26), i.e. the same dividing surface is used to define the TS with and without cavity, one can rely on the very good approximation that $K_{TST}^{(c)} \approx K_{TST}^{(0)}$.²⁶ As a consequence, the cavity effect on the rate follows directly from the ratio of the transmission coefficients

$$R = \frac{\kappa^{(c)}}{\kappa^{(0)}}. \quad (5)$$

Although $\kappa^{(c)}$ and $\kappa^{(0)}$ lie in the $[0, 1]$ range, the ratio R indicating the chemical rate enhancement or suppression can, in principle, be either larger or smaller than one.

Finally, it is important to define how to calculate the reactive flux with the expression in Eq. 4 when considering a molecular ensemble, since all coordinates of all molecules enter in the definition of the various quantities. In doing so, it is essential to realize that the fraction

of activated molecules (AM) F_{AM} , those which are undergoing the chemical transformation at a specific moment in time, to non-activated molecules (NAM) is in general very small. For a unimolecular reaction with a forward rate constant K and a total of N molecules coupled to the cavity, the rate of molecules that start the transformation per unit of time is $dN/dt = KN$. Multiplying by Δ_{TS} , the amount of time the molecule spends crossing the transition state (TS), and dividing by the total number of molecules N results in an estimate for $F_{AM} = K\Delta_{TS}$. Considering a rate of about 10^{-4} s^{-1} as in the example of Ref. 3, and with $\Delta_{TS} \approx 10^{-13} \text{ s}$ for a typical reaction in solution,³⁷ one obtains $F_{AM} \approx 10^{-17}$. A rate of 10^4 s^{-1} , of the order of the HONO isomerization studied here, results in $F_{AM} \approx 10^{-9}$, still negligible compared to the fraction of spectator NAMs. Hence, when considering the modification of chemical rates for ensembles under strong coupling, one must assume that on average only one AM crosses the barrier at a time. In our classical treatment of the reactive flux, this means that the sampling of transition state configurations according to Eq 4 is performed for one molecule only, while the other molecules are in thermal equilibrium close to their minimum energy configurations in the reactant potential energy well. Every set of different model parameters of the simulations studied below consists of a batch of 10^4 trajectories sampled from a canonical ensemble. The simulations are built on top of the OpenMM package for customizable molecular simulation.³⁸

The three spatial directions of the dipole in the body-fixed molecular frame along the reaction coordinate τ are shown in Fig 1b. The modulation of the μ_z component is very small as a function of τ and its largest modulation occurs instead in the stretching and bending modes of the molecular skeleton. The μ_z component of the dipole is the only one available from *ab initio* calculations. Hence, to be consistent, here we use a simple partial charge model of the dipole for its three components that agrees qualitatively well with calculated cuts of the *ab initio* dipole surfaces. Details are found in the supporting material.

We begin the discussion of the results by considering the effect of the cavity on an ensemble of N randomly oriented HONO molecules for $\omega_{cav} = 640 \text{ cm}^{-1}$, which is the

frequency of the reaction coordinate at the minimum-energy geometry of the *cis* potential well.²⁶ Fig 2a presents the transmission coefficient as a function of N for randomly oriented HONO molecules. Outside the cavity, $\kappa^{(0)} \approx 0.23$ at 300 K as can be seen in the black trace, Fig 2a, and also reported in Ref. 26. This relatively low transmission is caused by a slow rate of intra-molecular vibrational energy redistribution (IVR) from the reaction coordinate of the AM to the rest of the molecular system in the low friction regime. Now, for a single molecule ($N = 1$) inside the cavity we fix the coupling strength to $g = 0.4$ V/nm, smaller than the weakest coupling considered in Ref. 26, but still showing a clear enhancement of the chemical rate in line with the results reported there. Note, however, that now the single molecule is randomly oriented and its atomistic trajectories in Cartesian space include rotations and vibrations. Next, we consider $N = 64$, where one molecule corresponds to the AM while $N - 1$ are spectator NAMs. Rather than fixing the macroscopic Rabi splitting by multiplying the coupling strength with the $1/\sqrt{N}$ factor, we keep it constant to $g = 0.4$ V/nm. Hence, the AM is coupled to the cavity with the same coupling strength in both the $N = 1$ and the $N = 64$ cases. This way, the modification of the rate cannot be attributed to an artificial re-scaling of the cavity to single-molecule coupling, and can only be attributed to a genuine collective modification of the dynamics of the AM through the presence of spectators molecules. The latter are only indirectly coupled to the AM via the cavity mode. For $N = 64$, $\kappa^{(c)}$ is further enhanced, as seen by comparing the orange and blue curves in Fig 2a. The cavity plus NAMs further accelerate the chemical reaction by increasing the total transmission coefficient compared to $\kappa^{(0)}$ and to $\kappa^{(c)}(N = 1)$ i.e. $R > 1$.

In the following, we describe the mechanistic insights behind this numerical experiment. First of all, we must note that the reported effect stagnates at $N \approx 36$ for the choice of model parameters when considering $R(N)$ in Fig. 2b for the randomly oriented molecules. As such, the reported rate modification does not explain the macroscopically²⁰ large N limit, which remains a standing unresolved issue in the field, but which is not the focus of this contribution. We emphasize that it is not the goal of this paper to address the macroscopic

large N limit involving correspondingly small single-molecule couplings. Indeed, in the opinion of the authors, this limit likely escapes the framework provided by Hamiltonian 1, irrespective of whether it is considered quantum mechanically or by classical mechanics.

However, our simulations shed important light on the distinct roles played by the AM and NAMs in the few molecules, vibrational strong coupling regime. Thus, in the following our goal is to explain the mechanisms by which the added NAMs modify the reaction rate of the AM, even though the AM and NAMs are not directly coupled and only interact with each other indirectly through the cavity degree of freedom.

Let us first compare the simulations with randomly oriented initial conditions to simulations performed with aligned molecules. When all molecules have their x -axis (cf. Fig. 1) aligned with the cavity polarization the collective effect disappears, as illustrated by the orange trace in Fig 2b. In stark contrast, when the cavity polarization is aligned with HONO's y -axis, the enhancement of the reaction rate with increasing N is even more pronounced as compared with the randomly oriented case. Comparing the three cases, R is similar when $N = 1$ and a modification of the rate in the $N > 1$ case only occurs for randomly oriented and y -aligned cases. This observation indicates that the orientation of the molecules with respect to the cavity polarization can be very important, and that the AM and the $N - 1$ NAM (spectators) play different roles in connection with their orientation inside the cavity. Indeed, molecules with their x -axis oriented with the cavity polarization experience the largest modification of the permanent dipole as they cross the transition state region, blue trace in Fig. 1b. Therefore, the AM efficiently couples with the cavity in this orientation. The AM also couples efficiently with the cavity when its y -axis is oriented with the cavity polarization. Here, the most efficient coupling will occur when the AM visits the *cis* or *trans* regions of the configurational space (see orange trace in Fig. 1b), which occurs just a few femtoseconds before or after having passed the TS. This situation is radically different for the NAMs because their energy content along the reaction coordinate is thermal and much lower than the AM. Thus, they are confined to oscillate close to the potential energy

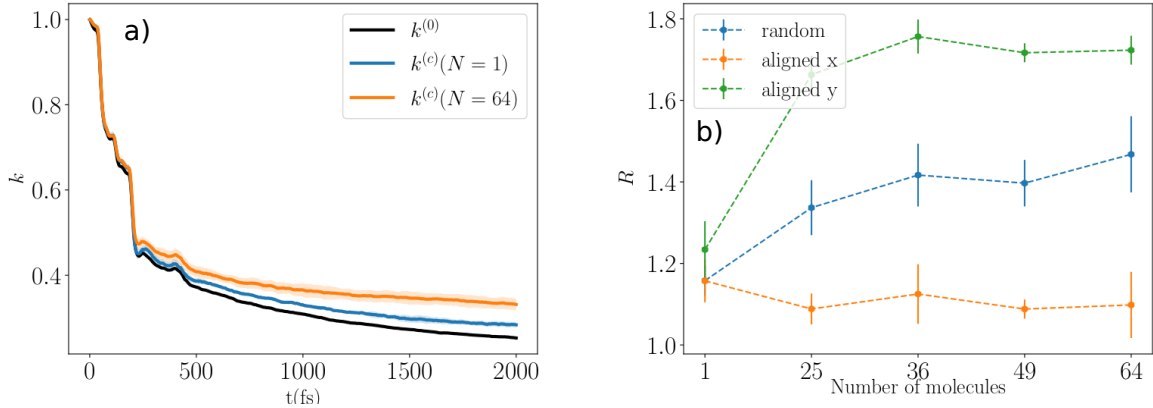


Figure 2: a) Transmission coefficient $\kappa^{(c)}(t)$ with fixed $g = 0.4$ (V/nm) with different N_{mol} , $\omega_{cav} = 640$ cm $^{-1}$ b) R for increasing number of molecules with fixed $g = 0.4$ V/nm (see text for details). Random case means that all molecules always randomly orientate when evolution. Aligned $x(y)$ molecules mean that the cavity polarization is aligned with HONO's $x(y)$ -axis and orientations of all HONO are fixed at all time.

minimum, where, in the case of HONO, $\partial\mu_x/\partial\tau = 0$. Thus, when the cavity is tuned to the frequency of the HONO torsion, only y -aligned NAMs can participate, whereas x -aligned NAMs are literally invisible to the cavity. Summarizing, both the AM and the $N - 1$ NAM must be efficiently coupled to the cavity for collective effects to take place, which may not necessarily occur for the same orientation, or even cavity frequency, as we illustrate below.

Once we have gained an understanding of the role of molecular orientation the question arises, through what specific mechanism do the NAMs participate in the modification of the chemical rate. Figure 3 shows R as a function of ω_{cav} from 400 cm $^{-1}$ to 800 cm $^{-1}$ (R in the ω_{cav} range 200 cm $^{-1}$ to 4000 cm $^{-1}$ is provided as SI). Interestingly, the rate modification peaks at a different frequency for the cases $N = 1$, ≈ 460 cm $^{-1}$, and $N = 64$, ≈ 520 cm $^{-1}$, with the single molecule case (necessarily the AM) being red-shifted by roughly 60 cm $^{-1}$. Considering the ratio of $R(N = 64)/R(N = 1)$ in Fig. 3b, one sees that the maximum collective effect peaks at $\omega_{cav} \approx 600$ cm $^{-1}$. These differences hint at the fact that the resonance condition between the cavity and the AM, which is the decisive element by which the rate can be modified, is modulated by the presence of the NAMs.

[change from here](#) To shed light on this matter, Fig. 4a compares the spectrum of the

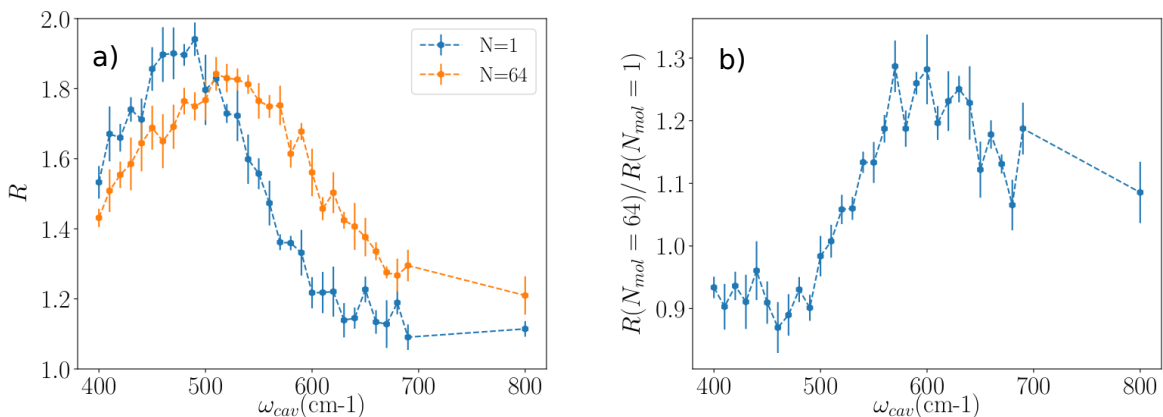


Figure 3: a) R for various cavity frequency from 400 to 800 cm^{-1} . $g = 0.4 \text{ V/nm}$ and $T = 300 \text{ K}$ for all calculations. b) A ratio of $R(N_{mol} = 64)$ and $R(N_{mol} = 1)$

velocity-velocity correlation function of the reaction coordinate, $I_{vv}(\omega)$, for AM and NAM i.e. for HONO trajectories sampled from a thermal distribution at the TS dividing surface, and for HONO molecules in thermal equilibrium around the *cis* configuration, respectively. Fig. 4a shows that the vibrational frequency of the AM along the reaction coordinate is red-shifted compared to the NAM, which is caused by the anharmonicity of the potential well along this coordinate and the higher energy content of the AM. Quantum mechanically, the anharmonic vibrational energy levels with the excitation localized along the reaction coordinate become closer, in particular $\tilde{\nu}_{01} = 632$, $\tilde{\nu}_{12} = 581$, $\tilde{\nu}_{23} = 555$, $\tilde{\nu}_{34} = 515$, and $\tilde{\nu}_{45} = 467 \text{ cm}^{-1}$,^{29,39} which classically results in a longer oscillation period at higher energy. The velocity-velocity spectrum of the NAM can be compared with the spectrum of the dipole-dipole correlation function,^{40,41} $I_{\mu\mu}(\omega)$, confirming that the peak at about 600 cm^{-1} in $I_{vv}(\omega)$ corresponds to the vibrational frequency of the NAM along the reaction coordinate. To validate the classical spectra we compare to an anharmonic quantum mechanical spectrum calculated with the MCTDH approach using the Heidelberg package,^{42,43} provided in the Supporting Material and showing qualitatively good agreement.

The blue-shifted vibrational frequency of the NAMs compared to the AM does not explain by itself the fact that, as the number of molecules increases, the largest rate modification occurs toward higher cavity frequencies. First, the AM should move off-resonance as ω_{cav}

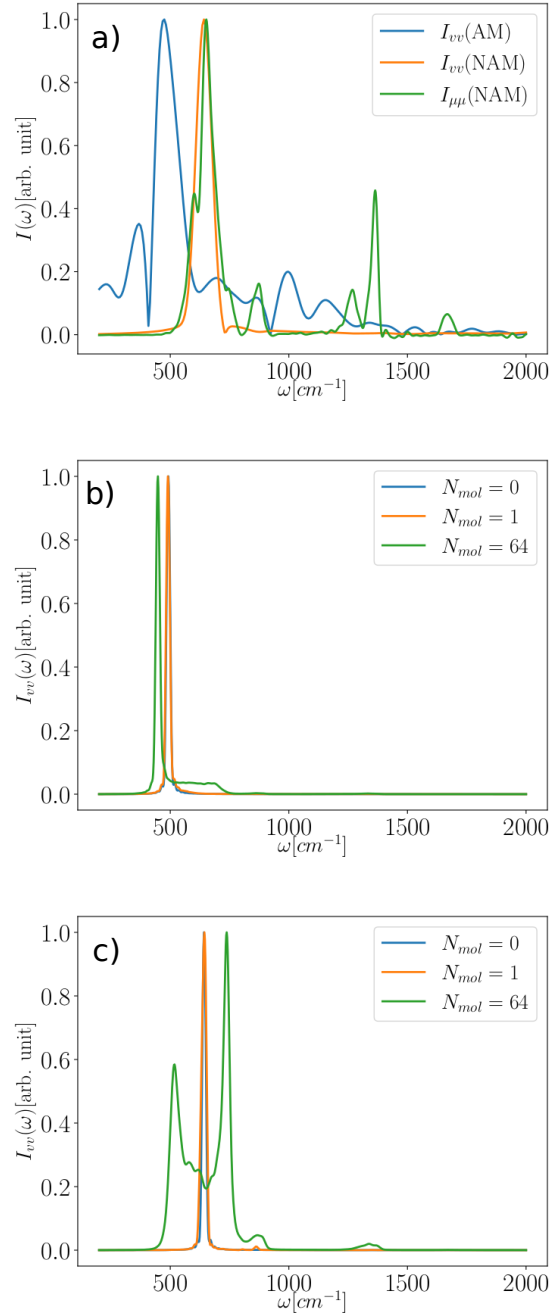


Figure 4: a) IR spectrum of non-activated HONO(NAM) and activated HONO(AM). The spectra are shown in absolute value. b) Velocity-velocity correlation spectrum of the cavity mode for $\omega_{cav} = 490$ cm^{-1} . c) Same as b) for $\omega_{cav} = 640$ cm^{-1} . $g = 0.4$ V/nm and $N_{mol} = 0, 1, 64$.

shifts to the blue. Second, the NAMs are not undergoing the chemical reaction, so the fact that their resonance condition improves with a blue-shifted cavity should, in principle,

not change the transmission coefficient of the AM. Figures 4b and 4c show the spectrum of the velocity-velocity correlation function, $I_{vv}(\omega)$, for the cavity mode for $\omega_{cav} = 490$ and 640 cm^{-1} , respectively, and for 0, 1 and 64 molecules in the cavity. At $\omega_{cav} = 490 \text{ cm}^{-1}$ and $N = 1$, $I_{vv}(\omega)$ presents a single peak at 490 cm^{-1} in all cases, without the formation of polaritonic peaks due to the relatively small single-molecule coupling, and with just a small red-shift for $N = 64$ (green trace in Fig. 4b). On the other hand, and in stark contrast, $I_{vv}(\omega)$ presents two polaritonic peaks for the $N = 64$ case and $\omega_{cav} = 640 \text{ cm}^{-1}$. Indeed, we want to emphasize that the single-molecule coupling strength is set such that no polaritonic branches exist for one single molecule, but such that they develop while increasing the number of molecules at fixed coupling from $N = 1$ to $N = 64$. Hence, at $\omega_{cav} = 640 \text{ cm}^{-1}$ the cavity is resonant with the NAMs and the collective coupling is strong enough to split the cavity frequency in an upper (UP) and lower polaritonic (LP) resonance. The LP is resonant with the red-shifted frequency of the AM, which leads to an efficient coupling and to the corresponding modification of the rate.

Thus, the following conclusions can be drawn: (1) For an effective modification of the rate in the single-molecule, strong coupling regime, the AM must be efficiently coupled and resonant with the cavity. This can be through the reaction coordinate directly, or through other modes anharmonically coupled to the reaction coordinate, as we have demonstrated previously.²⁶ (2) In the collective $N \gg 1$ strong-coupling regime, the AM must be resonant with vibrational modes of the cavity dressed by the NAMs, meaning for example resonances of the AM with polaritonic modes formed by the $N - 1$ spectators and the cavity.

One can still ask the question, what is the underlying physical mechanism by which the cavity plus NAMs change the reaction rate of AM. For this, we focus on the total energy variation of the AM after it has passed the transition state, $\Delta E = E(t) - E(0)$, as a function of time as plotted in Fig 5. The total energy of the cavity plus all molecules is divided into three subsystems, the AM, the NAMs and the cavity, and we consider the case for random molecular orientation. The energy barrier is about 4000 cm^{-1} or $20 k_B T$ at $T = 300 \text{ K}$.

The fastest energy loss from the AM occurs for $N = 1$ and $\omega_{cav} = 490$ cm-1, closely followed by $N = 64$ and $\omega_{cav} = 490$ cm-1 (blue and orange traces). The corresponding relative change in rate is $R = 1.9$ and $R = 1.8$, respectively (cf. Fig. 3b). The energy loss from the AM is slower at $\omega_{cav} = 640$ cm-1 than at $\omega_{cav} = 490$ cm-1. At $\omega_{cav} = 640$ cm-1, the $N = 64$ case loses AM energy faster than $N = 1$, since in the latter situation the resonance of the AM is largely detuned from the cavity, whereas for $N = 64$ the AM is resonant with the lower polaritonic state. The corresponding relative changes in the reaction rate are $R = 1.4$ and $R = 1.2$ for the $N = 64$ and $N = 1$ cases, respectively. Thus, the relative change in rate and the energy loss from the AM at short times are directly correlated. The better the AM is resonant with a mode of the cavity plus NAMs, the fastest the energy exchange of the AM with the rest of the system at short times after crossing the TS, and the largest the relative change in the chemical reaction rate. Only the energy transfer at short times is relevant, since $\kappa^{(c)}(t)$ reaches its plateau value when the AM becomes, in average, trapped in the reactant or product wells due to energy loss.

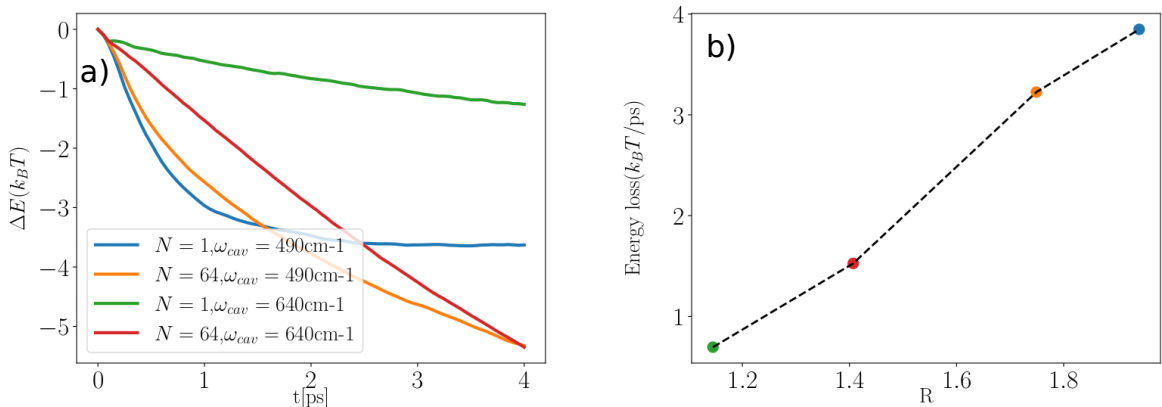


Figure 5: a) The energy difference, $\Delta E = E(t) - E(0)$, of AM as a function of time is plotted with $g = 0.4$ V/nm and $T = 300$ K for all calculations. b) The average energy loss, $E(t) - E(0)/t$, of AM within the first 0.5 ps is plotted as a function of R . The color of each point corresponds to the conditions shown in a).

Summarizing, we have investigated the effect of a cavity mode coupled to an ensemble of randomly oriented HONO molecules in the gas phase on the rate of the *cis-trans* isomeriza-

tion reaction. Our simulations demonstrate that the activated molecule, the molecule undergoing the chemical reaction at a given instant of time, and the ensemble of non-activated molecules, play fundamentally different roles. Specifically, the orientation with respect to the cavity that leads to the largest effect can be different for the activated molecule and the non-activated molecules. This is a consequence of the possible change of direction of the permanent dipole in real space for different configurations of the reacting molecule along the reaction coordinate in realistic systems. Also, the relevant resonances of the activated molecule that couple with the cavity may be shifted with respect to those of the non-activated molecules due to the much larger energy content of the former.

The largest modulation in the transmission coefficient occurs when the reaction coordinate (or a mode strongly coupled to the reaction coordinate²⁶) in the activated molecule becomes resonant with the cavity or a polaritonic resonance of the cavity with the non-activated molecules. This does *not* mean that the polaritonic resonance is already populated at room temperature before the chemical reaction takes place. It means that the polaritonic excited states can be populated through coupling to the activated molecule. Finally, the main mechanistic cause for the relative change in the transmission coefficient, $R = \kappa^{(c)}/\kappa^{(0)}$, is the average rate of energy loss from the activated molecule at short times, i.e. until $\kappa^{(c)}$ reaches its plateau value, which occurs due to the resonant coupling to the rest of the polaritonic system.

Our simulations cover the single-molecule to small-ensemble strong coupling regime in the gas phase, and therefore one should be cautious about extrapolating our results to the macroscopic limit of large N in Fabry-Perot cavity experiments. Strong coupling in the gas phase with methane molecules has recently been observed by the Weichman’s group,⁴⁴ and this could represent an interesting avenue for gas-phase experiments of cavity-modified molecular reactivity under well-controlled conditions, where solid mechanistic insights can be gained by the interplay of experiment and theory. Our findings shed important new light onto the question of collective effects in chemical reactivity under vibrational strong

coupling. However, it still remains for future work to better understand how these cavity effects can survive in actual liquid phases and in the collective regime for truly macroscopic numbers of molecules. We speculate that these answers might lie beyond the paradigm of non-interacting molecules with idealized cavity modes, and unveiling them may require studies of the transmission coefficient with full consideration of the molecular as well as electromagnetic environments.

Acknowledgement

J.S. is grateful to the International Max Planck Research School for Quantum Dynamics in Physics, Chemistry and Biology (IMPRS-QD) for financial support. We acknowledge financial support by the Deutsche Forschungsgemeinschaft (DFG) through project 429589046.

Supporting Information Available

Additional theoretical and numerical details including extra figures.

References

- (1) Hutchison, J. A.; Schwartz, T.; Genet, C.; Devaux, E.; Ebbesen, T. W. *Angew. Chem.* **2012**, *124*, 1624–1628.
- (2) Shalabney, A.; George, J.; Hutchison, J.; Pupillo, G.; Genet, C.; Ebbesen, T. W. *Nat Commun* **2015**, *6*, 5981.
- (3) Ebbesen, T. W. *Acc. Chem. Res.* **2016**, *49*, 2403–2412.
- (4) Dunkelberger, A. D.; Spann, B. T.; Fears, K. P.; Simpkins, B. S.; Owrutsky, J. C. *Nat. Commun.* **2016**, *7*, 13504.

- (5) Dunkelberger, A. D.; Davidson, R. B.; Ahn, W.; Simpkins, B. S.; Owrutsky, J. C. *J. Phys. Chem. A* **2018**, *122*, 965–971.
- (6) Yang, Z.; Xiang, B.; Xiong, W. *ACS Photonics* **2020**, *7*, 919–924.
- (7) Fassioli, F.; Park, K. H.; Bard, S. E.; Scholes, G. D. *J. Phys. Chem. Lett.* **2021**, *12*, 11444–11459.
- (8) Thomas, A. et al. *Angew. Chem. Int. Ed.* **2016**, *55*, 11462–11466.
- (9) Lather, J.; Bhatt, P.; Thomas, A.; Ebbesen, T. W.; George, J. *Angew. Chem. Int. Ed.* **2019**, *58*, 10635–10638.
- (10) Thomas, A. et al. *Science* **2019**, *363*, 615–619.
- (11) Vergauwe, R. M. A.; Thomas, A.; Nagarajan, K.; Shalabney, A.; George, J.; Chervy, T.; Seidel, M.; Devaux, E.; Torbeev, V.; Ebbesen, T. W. *Angew. Chem. Int. Ed.* **2019**, *58*, 15324–15328.
- (12) Thomas, A.; Jayachandran, A.; Lethuillier-Karl, L.; Vergauwe, R. M. A.; Nagarajan, K.; Devaux, E.; Genet, C.; Moran, J.; Ebbesen, T. W. *Nanophotonics* **2020**, *9*, 249–255.
- (13) Imperatore, M. V.; Asbury, J. B.; Giebink, N. C. *J. Chem. Phys.* **2021**, *154*, 191103.
- (14) Ahn, W.; Triana, J. F.; Recabal, F.; Herrera, F.; Simpkins, B. S. *Science* **2023**, *380*, 1165–1168.
- (15) Li, T. E.; Nitzan, A.; Subotnik, J. E. *J. Chem. Phys.* **2021**, *154*, 094124.
- (16) Li, X.; Mandal, A.; Huo, P. *Nat Commun* **2021**, *12*, 1315.
- (17) Li, T. E.; Nitzan, A.; Subotnik, J. E. *Angew. Chem. Int. Ed.* **2021**, *60*, 15533–15540.
- (18) Yang, P.-Y.; Cao, J. *J. Phys. Chem. Lett.* **2021**, *12*, 9531–9538.
- (19) Mandal, A.; Li, X.; Huo, P. *J. Chem. Phys.* **2022**, *156*, 014101.

- (20) Du, M.; Yuen-Zhou, J. *Phys. Rev. Lett.* **2022**, *128*, 096001.
- (21) Wang, D. S.; Neuman, T.; Yelin, S. F.; Flick, J. *J. Phys. Chem. Lett.* **2022**, 3317–3324.
- (22) del Pino, J.; Feist, J.; Garcia-Vidal, F. J. *New J. Phys.* **2015**, *17*, 053040.
- (23) Pérez-Sánchez, J. B.; Koner, A.; Stern, N. P.; Yuen-Zhou, J. *Proc. Natl. Acad. Sci.* **2023**, *120*, e2219223120.
- (24) Li, T. E.; Nitzan, A.; Subotnik, J. E. *J. Chem. Phys.* **2020**, *152*, 234107.
- (25) Campos-Gonzalez-Angulo, J. A.; Yuen-Zhou, J. *J. Chem. Phys.* **2020**, *152*, 161101.
- (26) Sun, J.; Vendrell, O. *J. Phys. Chem. Lett.* **2022**, *13*, 4441–4446.
- (27) Lindoy, L. P.; Mandal, A.; Reichman, D. R. *J. Phys. Chem. Lett.* **2022**, *13*, 6580–6586.
- (28) Nagarajan, K.; Thomas, A.; Ebbesen, T. W. *J. Am. Chem. Soc.* **2021**, *143*, 16877–16889.
- (29) Richter, F.; Hochlaf, M.; Rosmus, P.; Gatti, F.; Meyer, H.-D. *J. Chem. Phys.* **2004**, *120*, 1306–1317.
- (30) Montgomery, J. A.; Chandler, D.; Berne, B. J. *J. Chem. Phys.* **1979**, *70*, 4056–4066.
- (31) Rosenberg, R. O.; Berne, B. J.; Chandler, D. *Chemical Physics Letters* **1980**, *75*, 162–168.
- (32) Chandler, D. *Introduction to Modern Statistical Mechanics*; Oxford University Press: New York, 1987.
- (33) Berne, B. J.; Borkovec, M.; Straub, J. E. *J. Phys. Chem.* **1988**, *92*, 3711–3725.
- (34) Kuharski, R. A.; Chandler, D.; Montgomery, J. A.; Rabii, F.; Singer, S. J. *J. Phys. Chem.* **1988**, *92*, 3261–3267.

- (35) Eyring, H. *J. Chem. Phys.* **1935**, *3*, 107–115.
- (36) Hänggi, P.; Talkner, P.; Borkovec, M. *Rev. Mod. Phys.* **1990**, *62*, 251–341.
- (37) Gertner, B.; Whitnell, R.; Wilson, K.; Hynes, J. *J. Am. Chem. Soc.* **1991**, *113*, 74–87.
- (38) P, E. et al. *PLoS Comput Biol.* **2017**, *13*, 1005659.
- (39) Richter, F.; Gatti, F.; Léonard, C.; Le Quéré, F.; Meyer, H.-D. *J. Chem. Phys.* **2007**, *127*, 164315.
- (40) McQuarrie, D. A. *Statistical Mechanics*; University Science Books: Sausalito, California, 2000.
- (41) Nitzan, A. *Chemical Dynamics in Condensed Phases: Relaxation, Transfer and Reactions in Condensed Molecular Systems*; Oxford University Press, 2006.
- (42) Meyer, H.-D.; Manthe, U.; Cederbaum, L. *Chem. Phys. Lett.* **1990**, *165*, 73–78.
- (43) Beck, M. H.; Jäckle, A.; Worth, G. A.; Meyer, H.-D. *Phys. Rep.* **2000**, *324*, 1–105.
- (44) Wright, J. C. *Int. Rev. Phys. Chem.* **2002**, *21*, 185.